Integrated TiO_2 resonators for visible photonics

Jennifer T. Choy,* Jonathan D. B. Bradley, Parag B. Deotare, Ian B. Burgess, Christopher C. Evans, Eric Mazur, and Marko Lončar

School of Engineering and Applied Sciences, Harvard University, Cambridge, Massachusetts 02138, USA
**Corresponding author: jchoy@fas.harvard.edu*

Received November 14, 2011; revised December 21, 2011; accepted December 21, 2011; posted December 22, 2011 (Doc. ID 158143); published February 8, 2012

We demonstrate waveguide-coupled titanium dioxide (TiO_2) racetrack resonators with loaded quality factors of 2.2×10^4 for the visible wavelengths. The structures were fabricated in sputtered TiO_2 thin films on oxidized silicon substrates using standard top-down nanofabrication techniques, and passively probed in transmission measurements using a tunable red laser.

OCIS codes: 130.3120, 230.5750.

Optical microresonators are ubiquitous components in optical telecommunication systems and provide a compact means for studying cavity quantum electrodynamics [1]. The integration of microresonators into classical and quantum networks relies on materials that support high-quality optical components on a chip-scale [2,3]. In the growing field of quantum photonics, quantum emitters [4–6] operate primarily in the visible wavelengths. Therefore, the development of a chip-scale platform for the visible is a critical step toward the realization of quantum communication networks, and can be beneficial to classical applications, such as light generation and on-chip sensing. While gallium phosphide [7], silicon nitride [3,8,9], silicon dioxide [10], and diamond [11] are all promising materials, certain challenges remain, including intrinsic luminescence [8], difficulty of generating thin membranes with low optical loss [12], poor refractive index contrast with the surrounding medium [10], and low tolerance for fabrication imperfections due to inherently small characteristic lengths.

Titanium dioxide (TiO_2) can be added to the family of viable integrated visible photonics platforms. It is a wide-bandgap semiconductor (with a bandgap energy between 3–3.5 eV, depending on the crystalline phase [13]) with a moderately high index for the visible wavelengths ($n \approx 2.4$) and a wide transparency window from the near UV to the IR. It is also naturally abundant and is compatible with a host of conventional growth techniques. While the optical properties of TiO_2 have been exploited in three-dimensional photonic crystals [14], gratings [15], and waveguides [16,17], planar resonator structures in this material had yet to be demonstrated. Here we show scalable and integrable TiO_2 racetrack resonators, having loaded quality factors (Q) of the order of 10^4 with efficient coupling to a feeding waveguide.

Amorphous TiO_2 thin films of thickness 170 nm have been deposited on oxidized silicon substrates using RF sputtering of a Ti target in an O_2/Ar environment [17]. Prism coupling experiments [17] indicated that the deposited films have propagation losses as low as 2 dB/cm. These losses suggest that the material-limited Q for optical cavities is around 5×10^5. We used racetrack resonators since they allow for controllable coupling to a waveguide via the coupling length. The fabricated parameters were designed to minimize bending losses (by making bending radii $R = 30$ μm). Additionally, the waveguide–resonator separation g and coupling length L were chosen to ensure efficient transfer of light signal between the cavity and waveguide. To optimize the coupling, we set $g = 130$ nm and waveguide width $w = 250$ nm, and calculated the coupling efficiency as a function of L, using the difference between the effective indices of the even (n_e) and odd (n_o) eigenmodes of the coupled structure [18]. For the range of wavelengths between 630 and 640 nm, $L = 15$ μm provides near critical coupling for transverse electric (TE) polarized light.

We realized the designed structures using conventional top-down fabrication techniques, which include electron beam lithography on a positive electron beam resist (ZEP 520A), electron beam evaporation and liftoff of a chromium mask layer, and reactive ion etching in a CF_4/H_2 environment. The recipe has an etch rate of approximately 60 nm/min and leads to slightly slanted sidewalls with an angle of 75° [17]. The mask was subsequently removed by an etchant and polymer pads (SU-8 2002, with cross sections 3 μm × 3 μm) were written using electron beam lithography [19]. These pads overlap with the ends of the TiO_2 waveguides and extend to the edges of the chip [Fig. 1(a)]. The edges of the polymer waveguides were then cleaved to facilitate in- and out-coupling of light. The input and output facets are offset from one another to avoid direct scattering of uncoupled light into the collection fiber. The devices have surfaces with a roughness of around 10 nm and gaps of approximately 130 nm in the coupling regions [Fig. 1(b)–(d)].

We simulated the mode profiles of the fabricated devices [insets of Fig. 1(b)] using the finite element method (FEM). From Fig. 1, the waveguides have an etch depth of 150 nm and a width of 250 nm on their top facets. These dimensions support one fundamental mode in each of the TE and transverse magnetic (TM) polarizations with respective effective indices of 1.80 and 1.61 at a wavelength of 630 nm. The pedestal layer, which resulted from nonuniformity in our etching process, is roughly 20 nm thick and can be beneficial for waveguide-resonator coupling [3]. In our structure, this layer improves coupling into the TM-polarized modes, so that

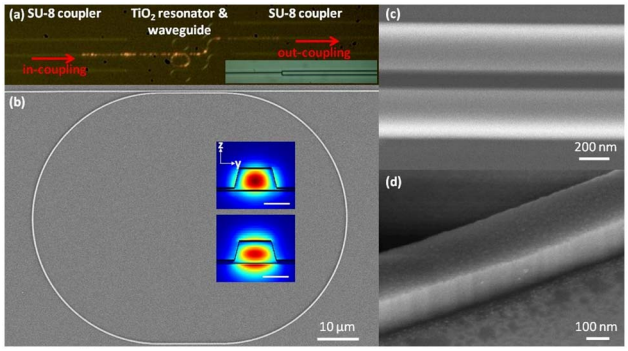

Fig. 1. (Color online) (a) Optical image of a set of TiO_2 waveguide-racetrack devices integrated with polymer pads. Inset: overlapping region between the TiO_2 waveguide and polymer pad. SEM images of (b) a TiO_2 waveguide-resonator, (c) its coupling region, and (d) etch profile taken at a 45° tilt. Insets: cross sections of the fabricated waveguide-resonator with simulated electric field profiles of the TE (top) and TM (bottom) modes. Propagation is in the x direction. Scalebar = 200 nm.

the simulated coupling efficiencies are around 90% for both TE- and TM-polarized light.

The resonators were characterized by transmission measurements using a tunable red laser with a scanning range of 634.4–639.6 nm. The output of the laser was coupled to a single mode, tapered lens fiber that was rotated such that the input signal into the sample was polarized along either the TE or TM direction. Light with a spot size of 0.8 μm in diameter was focused onto the facet of the polymer pad by the tapered lens fiber and transmitted into the waveguide-resonator device. The output was coupled through a polymer pad on the opposite end of the chip and collected by another tapered lens fiber that was connected to a high-speed silicon detector. For this experiment, the coupling loss from the fiber to the TiO_2 waveguide is roughly 14.5 dB at each end. This loss can be reduced by polishing the facets and optimizing the geometry of the TiO_2 waveguide to reduce light reflections that arise from the refractive index mismatch.

The resonator transmission spectra are shown in Fig. 2. All spectra shown here have not been normalized. The transmission spectra have periodically spaced dips corresponding to whispering gallery modes with either the TE [Fig. 2(a)] or TM [Fig. 2(b)] polarization. The small dips observed in Fig. 2(b) are due to imperfect polarization filtering of TE-polarized signals. The loaded quality factors ($Q_{\text{loaded}} = \frac{\lambda}{\Delta\lambda}$, where λ is the cavity resonance wavelength and $\Delta\lambda$ is the linewidth of the resonance) were extracted by fitting the transmission dips to the Fano model [20]. The model is necessary due to interference between the transmitted signals and partially reflecting elements in the waveguides, leading to asymmetries in the cavity line shapes [20]. The fits yielded linewidths as narrow as 0.028 nm and 0.11 nm for the TE and TM polarizations (respectively) near $\lambda = 635$ nm, corresponding to respective Q values of 2.2×10^4 and 5.6×10^3. The observed transmission drops are as large as 96%, indicating that the resonators are nearly critically coupled.

The transmission properties of a waveguide-coupled racetrack resonator have been well-described elsewhere [18,21]. The free spectral range (FSR) between consecu-

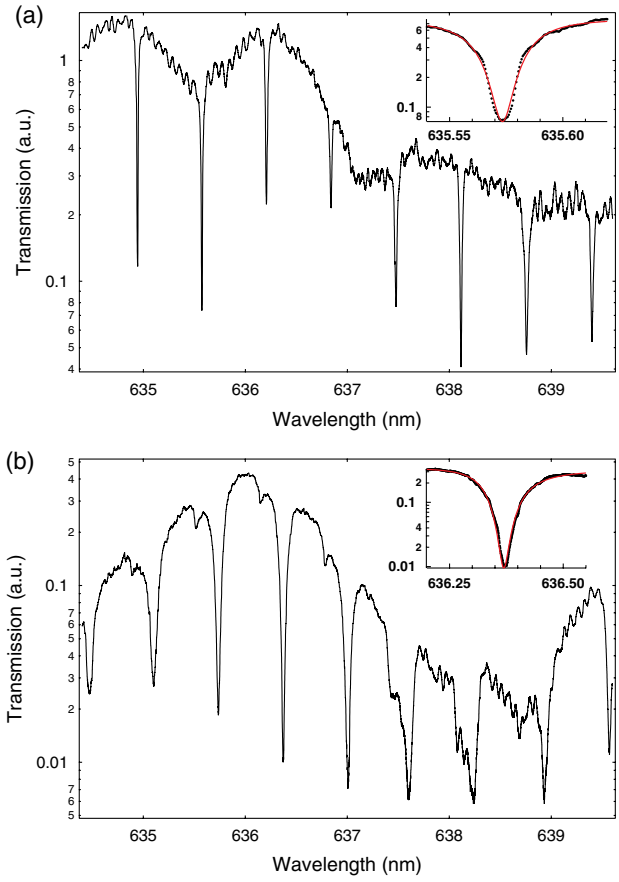

Fig. 2. (Color online) (a) TE-polarized transmission as a function of wavelength for a racetrack resonator with $R = 30$ μm and $L = 15$ μm. Inset: cavity mode at 635.57 nm, along with a fit to the Fano model (red). The fitted linewidth is 0.028 nm, corresponding to a Q of 22400. (b) TM-polarized transmission as a function of wavelength for the same resonator. Inset: cavity mode at 636.36 nm, with a fitted linewidth of 0.11 nm and corresponding Q of 5629.

tive modes in the system is described by $\text{FSR} \approx \frac{\lambda^2}{2n_g(\pi R+L)}$, where n_g is the group index and takes into account dispersion in the structure. We used the Sellmeier coefficients obtained from spectroscopic ellipsometry measurements on our TiO_2 films to determine the wavelength-dependent index (n_{mat}). The first-order effective index (n_{eff}) and group index (n_g) were then computed [22] and are shown in Fig. 3. In the visible wavelengths, n_g in TiO_2 waveguides can be significantly larger than n_{eff} (a difference of approximately 57% for the TE mode and 70% for the TM mode). The greater difference observed in the TM polarization is due to larger waveguide dispersion, which can be estimated by calculation of the group index $n_{g,w}$ of the given waveguide without considering the wavelength-dependence in n_{mat}. The large discrepancy between n_g and n_{eff} can thus be attributed to both waveguide and material dispersion, although the contribution from the latter decreases with increasing wavelengths, as indicated by the diminishing difference between the group index with and without material dispersion (n_g and $n_{g,w}$, respectively). Dispersion must therefore be considered when designing optical components in TiO_2 and can be exploited to generate

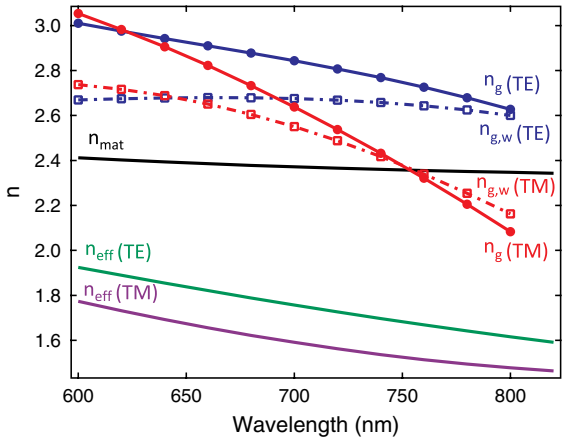

Fig. 3. (Color online) Calculated effective (n_{eff}) and group (n_g) indices as a function of wavelength for the TE- and TM-polarized waveguide modes. Contributions to the difference between n_{eff} and n_g include dispersions in the material (n_{mat}) and waveguide, which can be inferred by calculating n_g using a fixed n_{mat} of 2.4 ($n_{g,w}$).

small FSRs without significantly increasing the device footprint. The calculated n_g values are in good agreement with the experimentally obtained value, in which an FSR of 0.64 nm [Fig. 2(a)] corresponds to a group index of 2.92 in the 635 to 640 nm range in the TE polarization.

Finally, the propagation loss in a critically coupled resonator can be estimated using $\alpha_r = \frac{\pi n_g}{\lambda Q_{\text{loaded}}}$ [23]. Based on a TE-polarized mode with a Q of 22400 and transmission drop of 92% [inset of Fig. 2(a)], the corresponding propagation loss is 28 dB/cm. The deviation from the planar loss value can be attributed to scattering losses from surface roughness introduced by the fabrication process, which might be reduced by using a top-cladding material.

We have demonstrated planar resonators in TiO_2 thin films for visible light operation with efficient coupling to waveguides for delivering light on- and off-chip. The methods and devices shown here could help advance the TiO_2 material platform toward integration with active emitters for novel and integrated classical and nonclassical light sources and on-chip sensing.

The research described in this paper was supported by the National Science Foundation (NSF) under contract ECCS-0901469 and based upon work supported as part of the Center for Excitonics, an Energy Frontier Research Center funded by the U.S. Department of Energy, Office of Science, Office of Basic Energy Sciences under award DE-SC0001088. The devices were fabricated at CNS at Harvard University. We thank Q. Quan, B. Hausmann, M. McCutcheon, M. Khan, F. Parsy, L. Xie, G. Akselrod, V. Bulovic, M. Pollnau, R. Jensen, L. Marshall, and M. Bawendi for useful discussions and help with the project. J. Choy acknowledges support from NSF GRFP.

References

1. K. Vahala, Nature **424**, 839 (2003).
2. M. Lipson, J. Lightwave Technol. **23**, 4222 (2005).
3. E. S. Hosseini, S. Yegnanarayanan, A. H. Atabaki, M. Soltani, and A. Adibi, Opt. Express **17**, 14543 (2009).
4. C. Kurtsiefer, S. Meyer, P. Zarda, and H. Weinfurter, Phys. Rev. Lett. **85**, 290 (2000).
5. C. B. Murray, C. R. Kagan, and M. G. Bawendi, Annu. Rev. Mater. Sci. **30**, 545 (2000).
6. B. Lounis and W. E. Moerner, Nature **407**, 491 (2000).
7. K. Rivoire, A. Faraon, and J. Vuckovic, Appl. Phys. Lett. **93**, 063103 (2008).
8. M. Barth, N. Nsse, J. Stingl, B. Lchel, and O. Benson, Appl. Phys. Lett. **93**, 021112 (2008).
9. M. Khan, T. M. Babinec, M. W. McCutcheon, P. B. Deotare, and M. Loncar, Opt. Lett. **36**, 421 (2011).
10. Y. Gong and J. Vuckovic, Appl. Phys. Lett. **96**, 031107 (2010).
11. A. Faraon, P. E. Barclay, C. Santori, K.-M. C. Fu, and R. G. Beausoleil, Nature Photon **5**, 301 (2011).
12. C. F. Wang, R. Hanson, D. D. Awschalom, E. L. Hu, T. Feygelson, J. Yang, and J. E. Butler, Appl. Phys. Lett. **91**, 201112 (2007).
13. S. A. Campbell, H.-S. Kim, D. C. Gilmer, B. He, T. Ma, and W. L. Gladfelter, IBM J. Res. Dev. **43**, 383 (1999).
14. G. Subramania, Y.-J. Lee, A. J. Fischer, and D. D. Koleske, Adv. Mater. **22**, 487 (2010).
15. T. Alasaarela, T. Saastamoinen, J. Hiltunen, A. Saynatjoki, A. Tervonen, P. Stenberg, M. Kuittinen, and S. Honkanen, Appl. Opt. **49**, 4321 (2010).
16. M. Furuhashi, M. Fujiwara, T. Ohshiro, M. Tsutsui, K. Matsubara, M. Taniguchi, S. Takeuchi, and T. Kawai, AIP Advances **1**, 032102 (2011).
17. J. D. B. Bradley, C. C. Evans, J. T. Choy, O. Reshef, P. B. Deotare, F. Parsy, K. C. Phillips, M. Loncar, and E. Mazur are preparing a manuscript to be called "Submicrometer-wide amorphous and polycrystalline anatase TiO_2 waveguides."
18. M. K. Chin, C. Youtsey, W. Zhao, T. Pierson, Z. Ren, S. L. Wu, L. Wang, Y. G. Zhao, and S. T. Ho, IEEE Photon. Technol. Lett. **11**, 1620 (1999).
19. Q. Quan, P. B. Deotare, and M. Loncar, Appl. Phys. Lett. **96**, 203102 (2010).
20. S. Fan, Appl. Phys. Lett., **80**, 908 (2002).
21. L. Zhou and A. Poon, Opt. Express **15**, 9194 (2007).
22. A. Guarino, G. Poberaj, D. Rezzonico, R. Degl'Innocenti, and P. Gunter, Nat. Photon. **1**, 407 (2007).
23. K. Preston, B. Schmidt, and M. Lipson, Opt. Express **15**, 17283 (2007).